Conception of a compact flow boiling loop for the International Space Station- First results in parabolic flights

Paul Chorin, Antoine Boned, Julien Sebilleau, Catherine Colin, Olaf Schoele-Schulz, Nicola Picchi, Christian Schwarz, Balazs Toth, Daniele Mangini

INSTITUT DE FRANCE
Académie des sciences

Comptes Rendus
Mécanique

Paul Chorin, Antoine Boned, Julien Sebilleau, Catherine Colin, Olaf Schoele-Schulz, Nicola Picchi, Christian Schwarz, Balazs Toth and Daniele Mangini

Conception of a compact flow boiling loop for the International Space Station-First results in parabolic flights

Published online: 27 February 2023

https://doi.org/10.5802/crmeca.147

Part of Special Issue: Physical Science in Microgravity within the Thematic Group Fundamental and Applied Microgravity

Guest editors: Olga Budenkova (CNRS, Université Grenoble Alpes,Grenoble INP, SIMaP, 38000 Grenoble, France),
Catherine Colin (IMFT, Université de Toulouse, CNRS, INPT, UPS et GDR 2799 Micropesanteur Fondamentale et Appliquée) and Guillaume Legros (ICARE, CNRS UPR 3021, Univ. Orléans et GDR 2799 Micropesanteur Fondamentale et Appliquée)

Les Comptes Rendus. Mécanique *sont membres du Centre Mersenne pour l'édition scientifique ouverte*
www.centre-mersenne.org
e-ISSN : 1873-7234

Comptes Rendus
Mécanique
Published online: 27 February 2023
https://doi.org/10.5802/crmeca.147

Physical Science in Microgravity within the Thematic Group Fundamental and Applied Microgravity / *Sciences physiques en microgravité au sein du GDR Micropesanteur Fondamentale et Appliquée*

Conception of a compact flow boiling loop for the International Space Station- First results in parabolic flights

Paul Chorin [a], Antoine Boned [a], Julien Sebilleau [*, a], Catherine Colin [*, a], Olaf Schoele-Schulz [b], Nicola Picchi [b], Christian Schwarz [c], Balazs Toth [c] and Daniele Mangini [d]

[a] Institut de Mécanique des Fluides de Toulouse - Université de Toulouse - CNRS-INPT-UPS, Allée Camille Soula - 31400 Toulouse - France

[b] Airbus Defence and Space GmbH Claude-Dornier-Straße 88090- Immenstaad Germany

[c] European Space Agency ESTEC TEC-MMG Keplerlaan 1, PO Box 299 NL-2200 AG Noordwijk, The Netherlands

[d] cosine Remote Sensing BV Warmonderweg 14, 2171 AH Sassenheim, The Netherlands

E-mails: paul.chorin@toulouse-inp.fr (P. Chorin), antoine.boned@etu.toulouse-inp.fr (A. Boned), julien.sebilleau@imft.fr (J. Sebilleau), catherine.colin@imft.fr (C. Colin), olaf.schoele-schulz@airbus.com (O. Schoele), nicola.picchi@airbus.com (N. Picchi), christian.schwarz@esa.int (C. Schwarz), balazs.toth@esa.int (B. Toth), danymangini@msn.com (D. Mangini)

Abstract. The design of a pipe flow boiling experiment for the International Space Station is proposed, taking into account typical weight, power consumption and size constraints. The effect of singularities such as elbows upstream the test section is investigated. Velocity profiles downstream two elbows, measured by Particle Image Velocimetry are in good agreement with numerical simulation and allow to determine a specific distance (decay length) downstream the elbows for which the velocity profile recover its axisymmetry. From these results a breadboard is designed and tested in parabolic flights. Care has been taken to generate boiling downstream the decay length. Two-phase bubbly flow is observed with 2 perpendicular high-speed cameras in the test section and a symmetry of the bubble distribution in the pipe is verified for different gravity conditions when the bubbles are created after the decay length.

Keywords. Flow boiling, microgravity, Dean Vortex, Flow visualisation, bubbly flow.

Published online: 27 February 2023

* Corresponding authors.

1. Introduction

Gas-liquid and vapor-liquid flows are present in a wide variety of applications: vapor generator in thermal, nuclear or solar power plants for electricity production, transport of crude oil and natural gas mixture through long pipelines in petroleum industry. The chemical industries have utilized gas-liquid contactors to increase interfacial heat and mass transfers in absorption, stripping and distillation processes involving two-phase flow through complex geometries. Phase change in liquid-vapor systems is also beneficial for cooling of hot surfaces in steel industry or for the thermal management of electronic components. Two-phase flows are also present in space applications with the thermal control of the cryogenic upper stage tanks of the launchers, the chill-down of supplied lines by cryogenic liquid before engine re-ignition, thermal control of electronic components in satellites with loop heat pipes. Space exploration will also need the development and control of two-phase systems for energy production, propulsion of launchers, waste water treatment, operating in microgravity conditions but also in Moon or Mars gravity. Two-phase flow with phase change, boiling, condensation are complex phenomena, which combine heat and mass transfers, hydrodynamics, and interfacial phenomena. Furthermore, gravity affects the fluid dynamics and may lead to unpredictable performances of thermal management systems. From the 1960s onwards, the space industry has faced classic technical problems that stimulated the development of two-phase flow research at microgravity conditions. Among these are the predictions of flow pattern, pressure drop, heat transfer including critical heat flux and void fraction in thermo hydraulic systems. Beyond the design of space systems, reduced gravity two-phase flows can address some fundamental questions, which remain unsolved. On earth, due to the contrast of densities between the liquid and the vapor, the flow dynamics is often controlled by the gravitational force. As the gravity is suppressed, a new balance comes into play between inertial, viscous and interfacial forces so that the mechanics which govern the interactions between phases drastically changes. Low gravity conditions are particularly favorable to the emergence of surface tension as dominating force whose role is often small at 1g conditions except in microfluidic devices. Studies performed in the 1990s and early 2000s mainly concerned gas-liquid adiabatic flows, with the determination of the flow patterns and transitions [1–7], the measurements of void fraction or phase velocities [8], pressure drop [5, 7, 9]. From the beginnings of the 2000s the number of flow boiling experiments in tubes increased. Several results were reported on the detailed characterization of flow pattern and heat transfer coefficient including critical heat flux with different refrigerants R113, FC72, HFE7000, HFE7100 [10–20]. Several review articles have been published sumarising the main results: [5, 10, 12, 21–23]. Most of these experiments were performed in parabolic flights. However parabolic flights have some limitations due to g-jitter, that can affect the flow behavior at low mass flux. The time limitation of about 20s of microgravity is also too short to reach a steady state at low mass flux or a thermal equilibrium in metallic tubes. This observation has motivated the international space agencies to consider the opportunity to carry out flow boiling experiments on board the International Space Station.

A team of Japanese researchers developed the TPF (Two-Phase Flow) experiment in the KIBO module with the support of Japanese Space Agency JAXA. This experiment was operated onboard the International Space Station(ISS) during from July 2017 to March 2018, and from February 2019 to July 2019. Two series of flow boiling experiments with n-Perfluorohexane in a 4mm diameter tube were conducted in a metallic copper tube and in a transparent glass tube coating by a gold deposite. The data are under evaluation with a special care to the estimation of the heat losses for a precise evaluation of heat transfer [24].

An American experiment Flow Boiling and Condensation Experiments (FBCE) was launched to the ISS in August 2021. Flow boiling of n-Perfluorohexane in saturated conditions is under investigation in a rectangular channel of dimensions 114.6 mm heated length, 2.5 mm width, and

5 mm height. Two phase flows pattern, heat transfer and critical heat flux are studied. Results of ground experiments with a similar set-up are reported by the authors [25].

Europe is also considering the development of a two-phase flow loop to study flow boiling and condensation on board the ISS. The objective of this experiment would be to increase the range of studied parameters by comparison to the previous experiments and also to improve the diagnostics, with local time resolved measurements of the heat transfer, void fraction, wall and interfacial shear stresses and a careful characterization of the flow structure by high-speed video recording. The challenge for performing a flow boiling experiment in the ISS is to be able to implement the loop in a limited space with a limited power available. This motivated the European Space Agency to support a specific study to evaluate the implementation of a flow boiling loop with a test section consisting of a tube of 6 mm diameter in the European Drawer Rack 2 (EDR2). This study was performed in collaboration between the Institute of Fluid Mechanics of Toulouse and Airbus Defence and Space in Friedrichshaffen with the support of the European Space Agency. Due the space limitation, the distance between singularities (as elbows) and the test section is of course limited and a careful analysis has to be performed to insure that the flow will recover its axisymmetry in the test section where heat transfer, void fraction and wall shear stress are measured.

The second section of the manuscript is a detailed description of the context of the implementation of the loop: size of the container, power available, weight limitation which led to a first design of the loop. The single-phase flow hydrodynamics downstream 2 elbows is investigated by PIV measurements and by direct numerical simulations. The comparison of experimental and numerical results is presented and discussed in Section 3. In Section 4, a design of the two-phase flow loop for the ISS is proposed. This set-up has been operated on ground and in a parabolic flight campaign with microgravity and partial gravity conditions. In Section 5, some experimental results on the effect of gravity on the bubbly flow hydrodynamics are presented and discussed and the axisymmetry of the bubbly flow is checked.

2. Design of the experimental setup

The experimental setup, called CoSmo (compact small scale convection loop) aims to study the effects of gravity on the flow pattern and associated heat transfer in convective flow boiling in a tube of 6 mm internal diameter. As the CoSmo breadboard is designed for a typical accommodation on-board the ISS, taking EDR2 as a reference, it has to fulfil several constraints in terms of mass, dimension, power consumption (both to heat the fluid and to power the acquisition systems), cooling power (to condensate the fluid before the entrance of the pump) and has to be operated in a specific temperature range. Table 1 summarizes these constraints for the CoSmo breadboard.

Table 1. Maximum values of the CoSmo breadboard dimension, weight, power consumption, cooling power and operational temperatures for possible accommodation in the EDR2

Parameter	Constraints
Dimension (mm)	720x900x400
Mass (kg)	50
Power consumption (W)	1030
Cooling (W)	1030
Operational temperatures (°C)	27-69

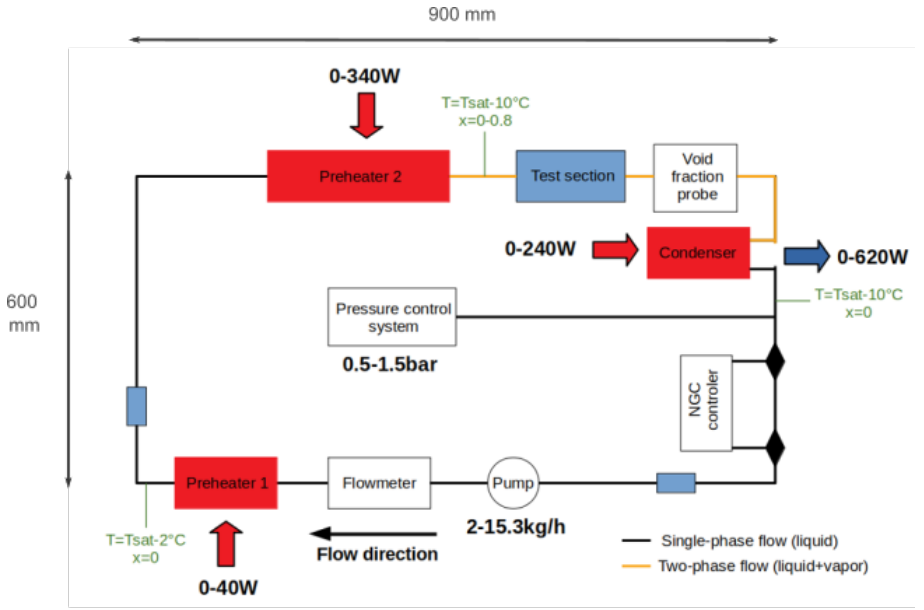

Figure 1. Scheme of the CoSmo breadboard.

Within the operational temperature range and power consumption constraint, n-perfluorohexane has been chosen as working fluid. Its moderate saturation temperature allows to work at various pressures (T_{sat} = 37.7°C at P = 0.5 Bar and T_{sat} = 68.9°C at P = 1.5 Bar) and of its low latent heat (L_v = 88 kJ.kg^{-1}) avoids too much power consumption for the boiling process. The density and dynamic viscosity of the liquid at 1 bar are ρ_l= 1619 kg.m^{-3} and μ_l=4.53 10^{-4} Pa.s, respectively. With this fluid, the range of parameters that can be achieved in the CoSmo breadboard are given in the Table 2.

Table 2. Parameters range in the CoSmo breadboard

Parameter	minimum value	maximum value
Mass flux G (kg.m^{-2}.s^{-1})	20	150
Thermodynamic vapor quality x	0.01	0.80
Pressure P (Bar)	0.5	1.5
Subcooling (K)	0	10

It can be noticed that the maximum mass flux (G = 150 kg.m^{-2}.s^{-1}) remains smaller but not so far from the value G = 200 kg.m^{-2}.s^{-1} where inertial effects become dominant compared to gravity effects [15]. The range of vapor quality allows to study the main flow patterns encountered in convective boiling namely bubbly, slug, churn and annular flows. In addition to the power consumption constraint, the CoSmo breadboard is also limited in its size. According to these constraints the typical scheme of the CoSmo breadboard is given in the Figure 1.

As one can see, the loop consists in two main part: a monophasic one from the condenser to the preheater 2 and a diphasic part (from the preheater 2 to the condenser) where the experiment on convective boiling is performed. Because of the dimension constraints, several elbows are present in the loop and we decided to keep a monophasic flow before the entrance of the Preheater 2, in order to avoid a liquid/vapor stratification in the elbows between the 2 preheaters.

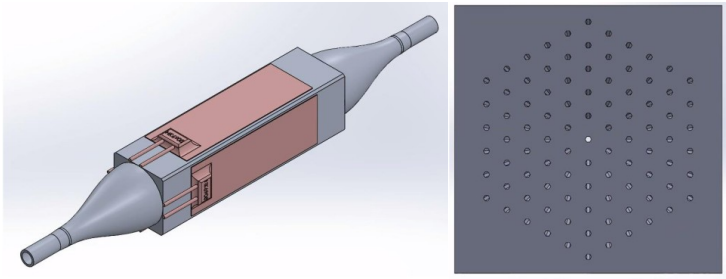

Figure 2. Scheme of the preheater 1 geometry and section.

At the outlet of the condenser, the fluid temperature is fixed at $T_{sat} - 10°C$ to avoid any cavitation in the pump. Due to the constraint of the maximum length (900 mm) it was not possible to vaporize all the fluid to the desired quality in preheater 2. Thus another preheater (preheater 1) was added after the flowmeter to heat up the fluid to $T_{sat} - 2°C$. This preheater has to be carefully designed in terms of length and heat flux to be able to reach the desired temperature with a sufficiently low heat flux to avoid boiling incipience. The maximum heat flux before the boiling inception was estimated thanks to the correlation of Frost and Dzakowic [26]:

$$\Delta T_{ONB} = T_p - T_{sat} = \sqrt{\frac{8\sigma \mathring{q} T_{sat}}{\lambda_L \rho_V h_{LV}} Pr_L} \tag{1}$$

where T_p is the wall temperature, σ the surface tension, λ_L the liquid thermal conductivity, ρ_V the vapor density, Pr_L the Prandtl number based on the liquid properties and $\mathring{q}$ the applied heat flux. Combining the Frost and Dzakovic correlation and the theoretical Nusselt number for laminar flow in tubes allows to determine the minimum length of heated tube to reach the desired temperature at the outlet of preheater 1. Unfortunately the calculated length was too large to be accommodated within the dimension restriction. Thus a specific design similar to a honeycomb structure was developed to allow to reach the desired temperature in a small length. The scheme of the preheater is illustrated in Figure 2. This preheater was manufactured thanks to a metallic 3D printing process and the heat is provided by four flat MINCO heating elements on its surface. Even if the flow is supposed to be monophasic between the two Preheaters, the elbows perturb the flow and can give rise to Dean vortices that break the axisymmetry of the flow in the preheater 2. It can result in undesired segregation of vapor bubbles in the bubbly flow regime. Thus the monophasic flow and the minimum length to retrieve an axisymmetric flow in the test section has to be studied prior the building of the CoSmo breadboard. This has been done both with numerical simulation and PIV measurements that are presented in the next section.

3. Single-phase flow qualification

As mentioned in the previous section, prior to the building of the CoSmo breadboard, the monophasic flow in the loop has to be studied to ensure that the flow at the entrance of the test section is axisymmetric and avoids bubble segregation in the bubbly flow regime. As the preheater 2 and the test section are downstream two elbows, a secondary flow induced by the curvature of the elbows can develop and break the axisymmetry. This secondary flow known as Dean vortices has been studied since the 1870's by Thomson [27–29]. Monophasic flows in curved pipes are parametrized with the pipe-to-curvature radii ratio $\delta = \frac{r}{R}$ (r being the pipe radius and R the radius of curvature of the pipe) and the Reynolds number $Re = \frac{2U_x r}{\nu}$ (U_x being the mean

flow velocity and ν the viscosity) and the secondary flow is generally parametrized thanks to the Dean number $D = Re\sqrt{\delta}$. Even if numerous studies have been devoted to classify the secondary flow with the Dean number, the decay length (minimum length to recover an axisymmetric flow after the curved part) has received less attention and the results mainly concern a U-bend [30–33]. Thus, to assess the proposed geometry for the CoSmo breadboard, both numerical simulations with OpenFOAM and PIV measurements have been performed to ensure that the flow at the entrance of the test section remains axisymmetric for the mass fluxes of interest $G \leq 150$ kg.m^{-2}.s^{-1} that corresponds to Reynolds numbers $Re \leq 2063$. According to Spedding et al. [34], with $\delta = 0.01$ which is the value proposed for the CoSmo breadboard the critical Reynolds number for transition to turbulence is $Re_c = 4838$ and thus a laminar flow is expected.

3.1. *Numerical simulations*

The numerical simulations have been performed with OpenFOAM using the simpleFoam solver that is adapted for laminar flows. The Semi-Implicit Method for Pressure Linked Equations (SIMPLE) algorithm is used for the pressure-velocity coupling. The gradient and laplacian terms are evaluated by central differencing scheme and the divergence terms by an upwind-biased scheme. All the spatial derivatives are second-order accurate. For each time step during the transient regime up to the converged steady state, the residuals fall below 10^{-8}. As the middle plane of the bend is a symmetry plane of the flow, only the upper half of the pipe is considered which enables to reduce the mesh size by a factor two. Thus, a symmetry condition on all variables is consequently set as a boundary condition for the middle plane. Within these parameters, the simulation have been tested on a single elbow configuration, depicted in Figure 3 **(a)**, that has been studied both numerically [35] and experimentally [36] for $Re = 700$ and $\delta = \frac{1}{6}$.

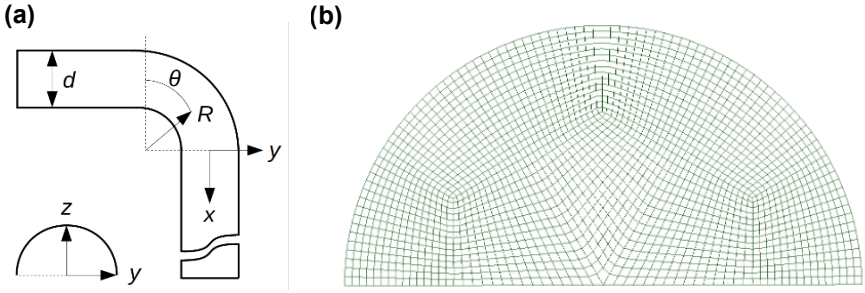

Figure 3. **(a)**: Scheme of the elbow and typical notation, **(b)**: mesh used in the simulation.

To prevent any disturbance at the entrance of the elbow, a small straight pipe of length 5d is added upstream the bend entrance. At the entrance of this 5D length pipe, a fully developed laminar velocity profile is imposed. A grid convergence is applied in this situation and it appears that a mesh with $N_{sect} = 8100$ cells per section and $N_{ax} = 12$ sections along the pipe per length of 6 mm (one pipe diameter) is sufficiently fine to obtain converged results. Figure 4 shows comparison of our results with those from literature at several positions in the elbow (i.e. at different θ values).

As one can see, a pretty good agreement is found with the experiments and previous numerical analysis. Numerical simulations were then performed on the CoSmo breadboard geometry from the entrance of the first elbow to the straight pipe at the exit of the second elbow to measure the flow profile and the decay length. The results are provided with the one obtained with the PIV measurements later in the text.

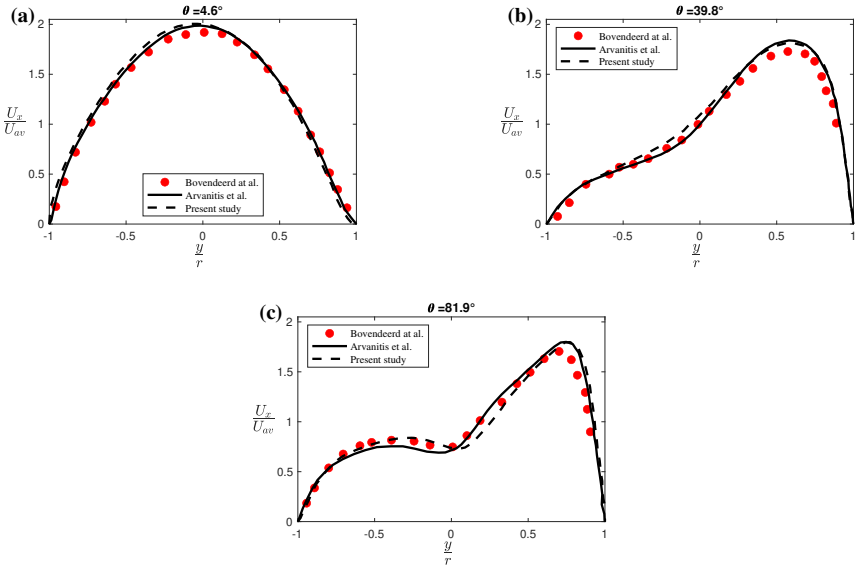

Figure 4. Comparison of the numerical results with the literature at position: **(a)**: $\theta = 4.6°$, **(b)**: $\theta = 39.8°$ and **(c)**: $\theta = 81.9°$.

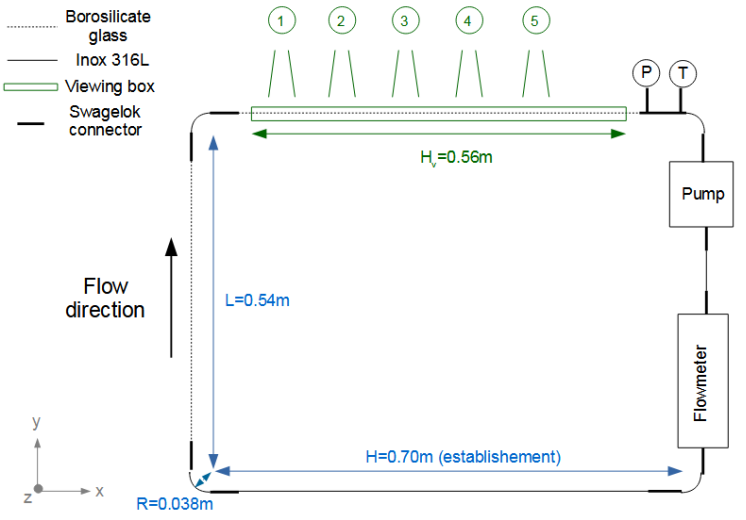

Figure 5. Scheme of the experimental setup used for PIV measurements

3.2. *PIV measurements*

To perform PIV measurement in a tube of 6 mm inner diameter, a specific test loop, with the same dimensions as the CoSmo breadboard, has been developed and is illustrated in Figure 5. To avoid severe optical distorsions linked to the small diameter of the tube, the measurement section is made of a tube in borosilicate glass inside a rectangular viewing box whose walls are also in borosilicate. Then, using an aqueous solution of potassium thiocyanate as working fluid

(and for filling the viewing box) allows to match the refractive index of the fluid and the glass [37] and to perform PIV measurement in both the horizontal and vertical middle plane of the tube. The borosilicate glass (from Schott) has a refractive index close to 1.47. Then to achieve index matching we use an aqueous solution with 64% of potassium thiocyanate in mass. According to Agrawal et al. [38] this solution has a density of 1384 kg.m^{-3} and a kinematic viscosity of 1.78 10^{-6} m^2.s^{-1}. As this fluid is corrosive, great care has been taken in the choice of the materials used in this loop. To achieve a Reynolds number up to $Re = 2000$ with this loop, an Iwaki MDG-M4 gear pump was chosen and the mass flow rate was measured with a Coriolis Bronkhorst M15 flowmeter. The PIV measurement were performed with a PCO DIMAX camera with a maximal resolution of 2000x2000 and the measurement plane was illuminated with Nd-Yag laser (532nm wavelength) of maximal 20W power. An optic device (from LaVision) generates a laser sheet 120μm thick and 3.2cm wide. The particles used as tracers were particles of glass covered with silver (average diameter 10μm, density 1400kg/m^3 close to the one of the fluid). Four Reynolds numbers ($Re = 500$, $Re = 1000$, $Re = 1500$ and $Re = 2000$) were tested and Bazus displacement bench allowed to move both the camera and laser to explore several locations as depicted in Figure 5.

3.3. *Decay length*

Figures 6, 7 and 8 present comparisons between the PIV measurements and the numerical results for several axial positions for $Re = 1000$, $Re = 1500$ and $Re = 2000$ respectively. The results for $Re = 500$ are not presented because both experiments and numerical simulations give a fully developed profile (i.e. Poiseuille flow) at the entrance of the viewing box.

As one can see, the numerical results and the PIV measurements gives very close results for $Re = 1000$ and $Re = 1500$ and the flow recovers an axisymmetry at a given distance downstream the second elbow allowing to measure a decay length L_d. The decay length is defined as the length downstream the second elbow at which the flow recovers its axisymmetry corresponding to a maximum of the velocity profile located at a distance of the tube axis smaller than 0.05 d, d being the tube diameter. For $Re = 2000$, the experiments shows a flow profile that appears flatter than the one predicted by the numerical simulations. This may results from a transition to turbulence in our experiments while the simulations were performed for a laminar regime. Nevertheless, the flow profile still recovers an axisymmetry downstream the second elbow and still allows to measure the decay length.

This decay length for both PIV measurements and numerical simulation is presented in Table 3. As one can see the good agreement between PIV measurements and numerical simulations is confirmed except for $Re = 2000$ (due to the transition to turbulence mentioned before). Theses values are of interest for the development of the CoSmo breadboard as having an axisymmetric flow to avoid bubble segregation in bubbly flow regime is a scientific requirement for the study of convective boiling under various gravity conditions.

Table 3. Decay length values from PIV measurements and from numerical simulations.

Re	L_d (cm) from PIV	L_d (cm) from numerics	$\frac{L_d}{d}$ from PIV	$\frac{L_d}{d}$ from numerics
500	14	13	23	22
1000	24	28	40	46
1500	51	46	85	77
2000	19	>60	32	>100

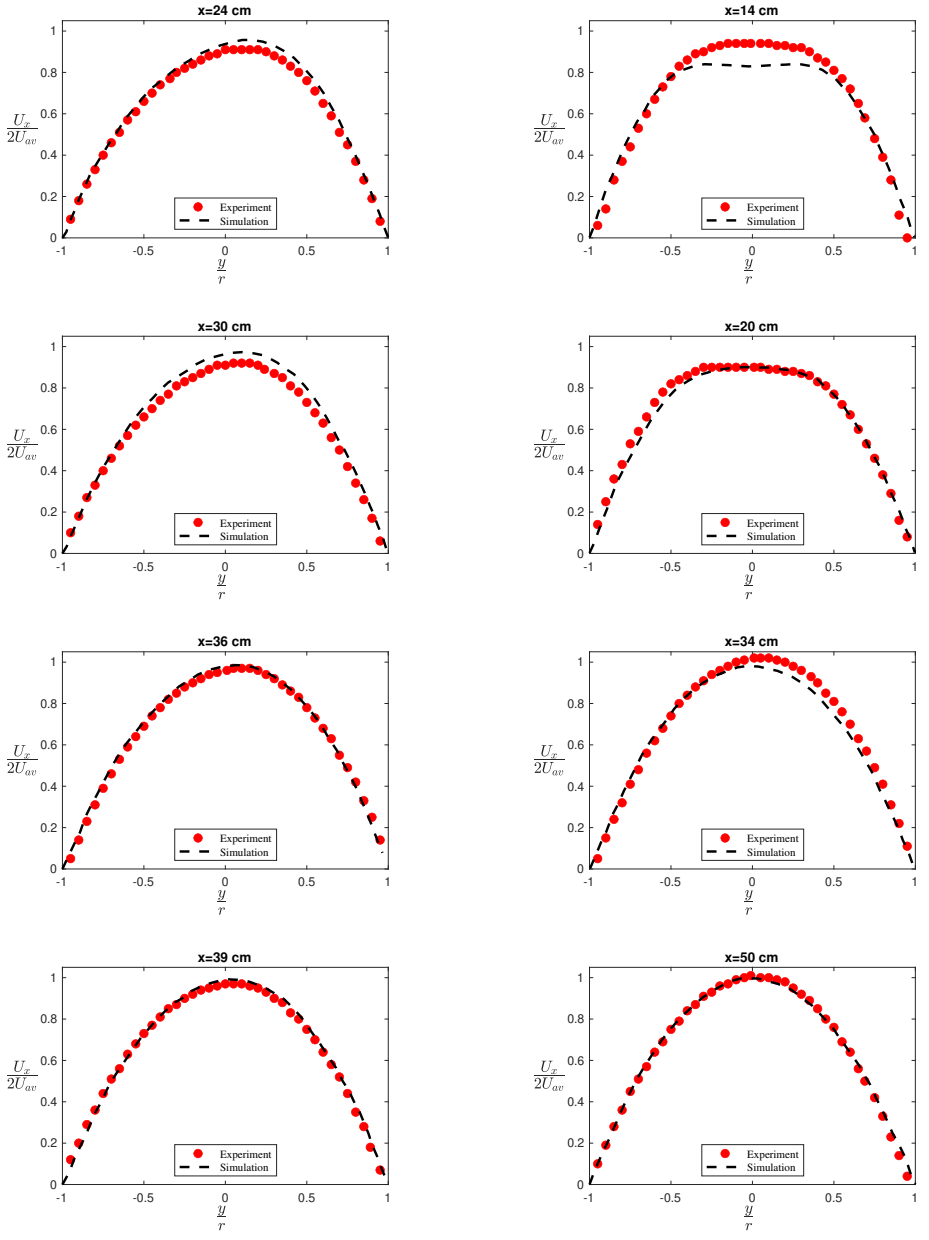

Figure 6. Comparison between the PIV measurement and the numerical simulation for $Re = 1000$ at various axial location. Left plots present experiments and simulations in the horizontal mid plane while right plots present experiments and simulations in the vertical mid plane.

4. Implementation of the CoSmo breadboard in parabolic flight and qualification

4.1. *Description of the CosMo loop*

Based on the previous results on the flow qualification downstream the elbows, a design of the CoSmo breadboard (Figure 9) with a 6mm inner diameter tube has been proposed. The size,

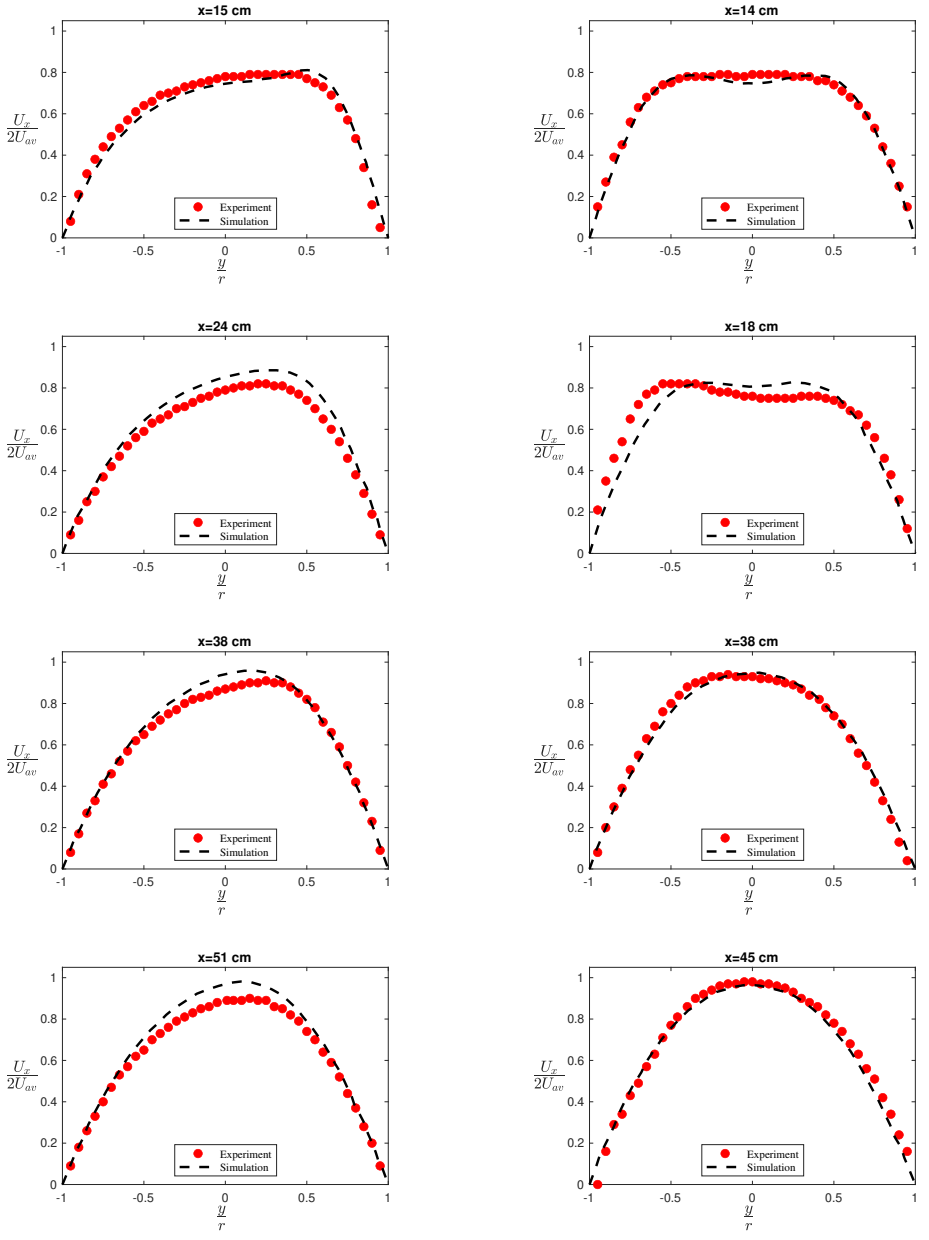

Figure 7. Comparison between the PIV measurement and the numerical simulation for $Re = 1500$ at various axial location. Left plots present experiments and simulations in the horizontal mid plane while right plots present experiments and simulations in the vertical mid plane.

weight and power consumption are compatible with an implementation in typical ISS payload racks, i.e EDR2 (see Table 1). In order to check the functionality of the loop in a microgravity environment, we first implemented it in a dedicated rack to participate to a parabolic flight campaign onboard the Airbus ZeroG Aircraft. The loop consists of a micro-annular gear pump

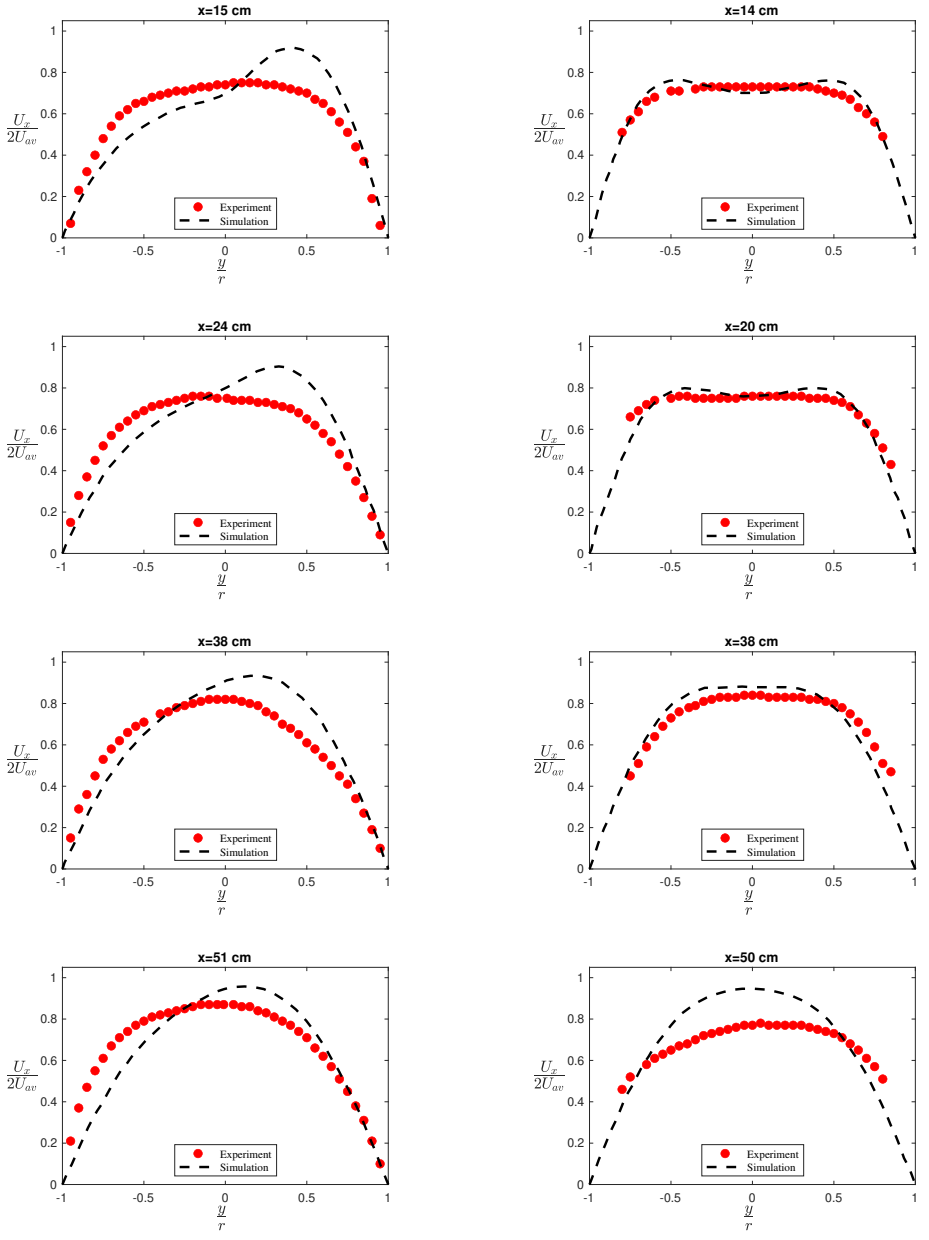

Figure 8. Comparison between the PIV measurement and the numerical simulation for $Re = 2000$ at various axial location. Left plots present experiments and simulations in the horizontal mid plane while right plots present experiments and simulations in the vertical mid plane.

model mzr-7265 from HNP Mikrosysteme operating with mass flux G up to 150 kg.m^{-2}.s^{-1}, a Coriolis flowmeter Bronkhorst M14, the preheater 1 (Figure 2), a straight line between the 2 elbows at the bottom part, the preheater 2 dowstream the second elbow, the test section, a void fraction probe, a condenser. The part of the loop between the preheaters 1 and 2 is the same as

the one of the loop for PIV measurements (Figure 5). The preheater 2 is a copper tube of 320 mm length, 6 mm inner-diameter and 10 mm outer-diameter with spiral grooves of 1mm depth. Due to size constraint, the length of the Preheater 2 has to be limited. The tube is heated by 3 wires (length 500 mm, diameter 1 mm) from Thermocoax, spiral rolled around an extruded copper cylindrical tube, providing each a maximal power of 110 W, allowing to reach a quality x up to 0.8. Each of the wire can be supplied independently, mentioned as PH2.1, PH2.2, PH2.3. For experiments at low quality values, especially for bubbly flow regimes, only the third wire farthest from the elbow (PH2.3) was used to let the flow recover its axisymmetry before nucleating the bubbles. PH2.1 is located between 7 cm and 18 cm downstream the elbow, PH2.2 from 18 cm to 29 cm and PH2.3 from 29 cm to 40 cm. For higher qualities values and the highest mass fluxes, the 3 wires were used. At the outlet of the test section, the two-phase flow enters the condenser composed of a cold plate with parallel mini channels. It is condensed and cooled down to a temperature of 10°C below the saturation temperature. On the external surface of the cold plate, 8 Thermo-Electric Coolers (TEC RC12-9 from Marlow) allow to extract a power up to 620 W. Series of fins (or heat sink) are placed above the TEC. Fans located above the fins allow to significantly increase the thermal dissipation. The pressure in the loop is set between 0.5 bar and 1.5 bar by a pressure control system designed and built by Airbus DS. The PCS consists of a metal membrane bellow that separates the fluid loop side chamber and the gas side chamber; the fluid side is assumed incompressible, therefore, its pressure can be controlled by regulating the pressure on the gas side. In order to avoid the need for a gas reservoir, the gas side chamber of the PCS is connected to a Diaphragm pump that can suck or inject air in the gas chamber. For laboratory and parabolic flight experiments, the experimental setup was placed vertically. The axis of the Preheater 2 and the test section was aligned with residual gravity, perpendicular to the floor (both in laboratory and in the aircraft).

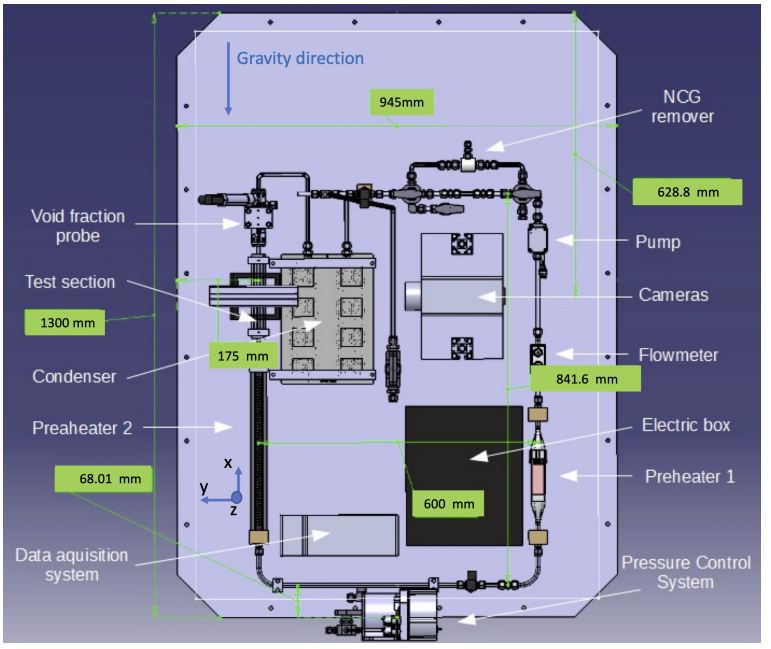

Figure 9. Scheme of the CoSmo loop for the parabolic flight campaigns.

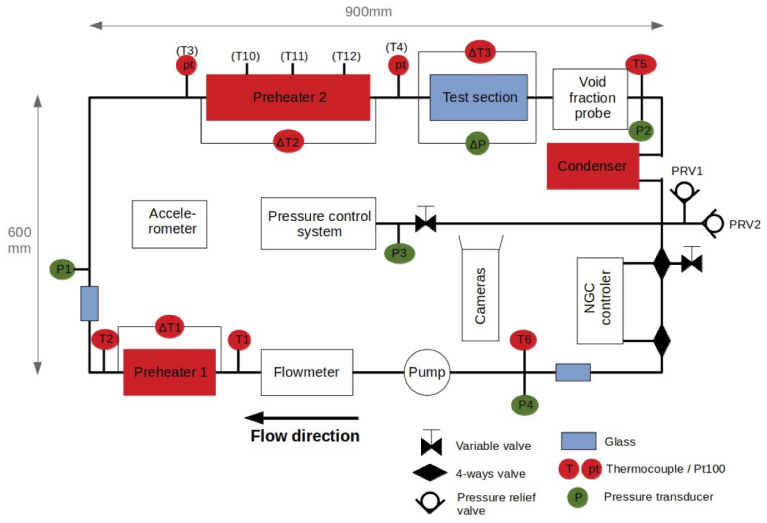

Figure 10. Location of thermocouples, pressure transducers in the CoSmo loop.

4.2. *Measurement technics*

Several Type K thermocouples and Pt100 probes are located all along the loop to measure the fluid temperature (T1 to T6), and the wall temperature of the preheater 2 (T10 to T12) (see Figure 10). Two Differential type T thermocouples allows to measure temperature difference along the 2 preheaters, for a precise thermal balance. Thanks to these thermocouples it was possible to quantify the heat losses and to measure the quality x at the entrance of the test section as described in [15]. The pressure at different locations in the loop (P1 to P4) is measured with four absolute pressure transducers (Keller 0-5 bars) and the pressure drop in the test section by a differential pressure transducer Validyne. An accelerometer is also used to record the residual acceleration along the 3 axis of the Aircraft during the flight. The void fraction probe, is a capacitance probe giving an averaged value of the capacitance of the liquid-vapor mixture which can be related to the void fraction after experimental or numerical calibration. Description of this probe can be found in [15]. All the measurements are acquired by the Data Acquisition system Ni-DAQ Compact Rio and recorded on a laptop. An interface for the control of the loop and the data acquisition, has been developed using Labview software.

4.3. *Test section and flow visualizations*

The test section is used for the visualizations of the two-phase flow and to assess the axisymmetry, especially in the bubbly flow regime. This test section is adiabatic and 12 cm long. It is a borosilicate glass tube of 6mm inner diameter and 8 mm outer diameter surrounded by a rectangular glass box. Two cameras PCO 1200 HS (16bit gray scale images size of 1280x401pixels with a spatial resolution of 30 pixels/mm and a frame rate of 400Hz) are used to film the flow in two perpendicular planes. The two cameras are placed one above the other and a mirror reflects one of the views. Camera 2 recorded images of the flow in the plane (x,y) in Figure 9 and Camera 1 in the plane (x,z) in Figure 9. Two backlights are placed on the opposite side of the cameras for homogenous and parallel backward illumination. They allow to have a good contrast in the images and to ease the detection of the bubble contours. The visualization box is filled with glycerin to reduce optical distortion. The index of refraction of the glycerin and

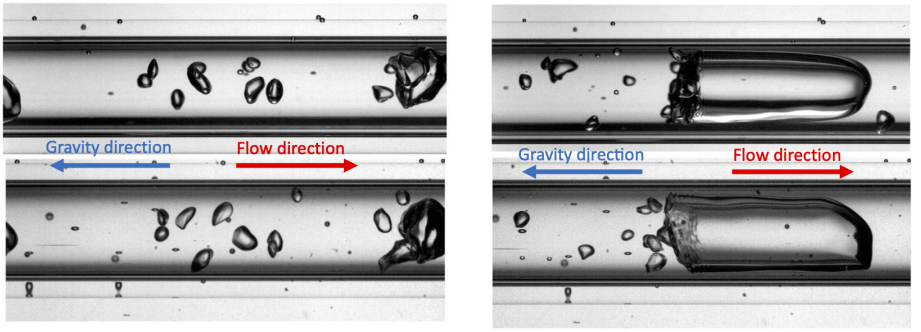

Figure 11. Flow visualization in earth gravity with the 2 perpendicular cameras (top camera 1, bottom camera 2): left bubbly flow G=20kg/m^{-2}.s^{-1} and x=0.01, right slug flow G=80 kg/m^{-2}.s^{-1}, x=0.06.

the glass are the same and equal to 1.47 and the index of refraction of the fluid FC72 is 1.23. The optical distortion was measured with a grid target of points regularly spaced of 0.125 mm. No distortion was observed in the area between -2 and +2mm from the pipe axis. Nevertheless, optical distorsion was observed very close to inner wall of the tube. It is visible on the images with the black bands in the vicinity of the inner wall. Synchronized images of the two cameras are acquired with the Cameware software on a computer. An example of bubbly flow and slug flow visualisation is given Figure 11.

4.4. *Parabolic flights*

For the parabolic flight campaign, the experimental set-up was accommodated into 2 racks: one containing the fluid loop and electronics in a double containment (Rack 1) and one is the “control Rack” (Rack 2) containing the electrical supplies and 3 computers for data and image acquisitions. It is operated by three people (see Figure 12). The 76th ESA Parabolic Flight Campaign took place in Paderborn (Germany) from 25th to 30th June 2021, with 3 flights of 31 parabolas each. It was a partial gravity campaign with 31 parabolas in microgravity, 31 parabolas in Moon gravity (0.16g) and 31 parabolas in Mars gravity (0.38g). The periods of partial gravity were at least 20 s long. Experiments were performed with 3 mass fluxes G=50, 100 and 150 kg/m^{-2}.s^{-1}, corresponding to liquid Reynolds numbers Re_l of about 650, 1300 and 2000, respectively and qualities x up to 0.4.

5. First results of the parabolic flight campaign

The main objective of this parabolic flight campaign was to assess the axisymmetry of the two-phase flow in the test section in microgravity conditions. Unfortunately, for this campaign, only PH2.1 the first part of the Preheater 2 worked, due to an electrical failure. The single-phase flow recovered its axisymmetry only at the end of PH2.1 for G= 50 kg/m^{-2}.s^{-1}. It means that for the mass fluxes G= 100 and 150 kg/m^{-2}.s^{-1}, the bubbles were produced in the preheater 2 at a distance from the elbow where the single-phase flow did not recover its axisymmetry. From the flow visualisations with the two perpendicular cameras, the radial distribution of the bubbles was investigated and compared to some results obtained on ground. Another target for this parabolic flight campaign, was to point out the influence of the residual gravity on the bubbly flow.

Figure 12. Operators during pre-flight preparation in front of the control rack (Rack 2), in the background the experimental rack (Rack 1); interior of the AirZero-G A310 aircraft

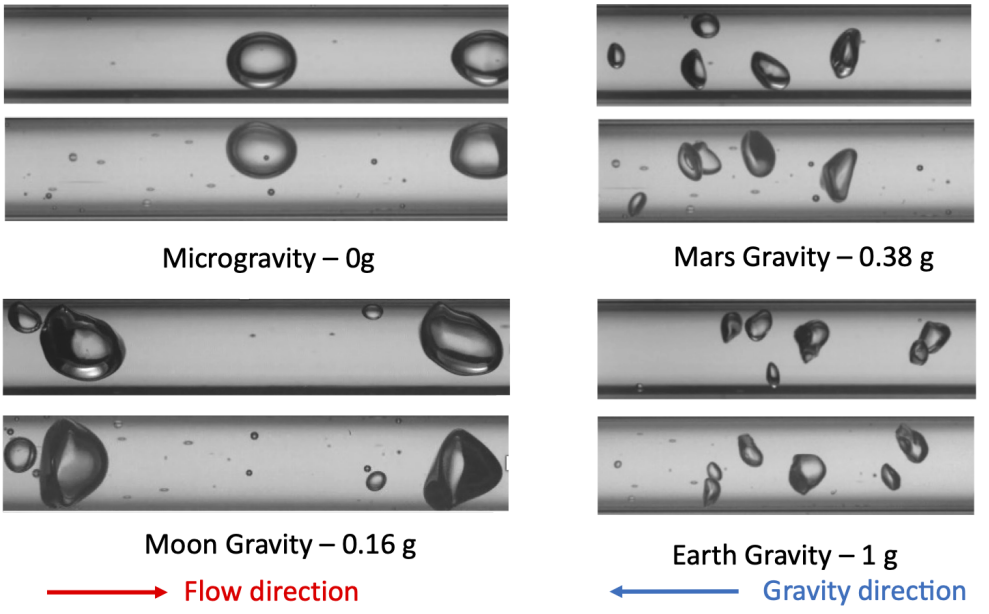

Figure 13. Flow visualizations with the 2 cameras for G=100 kg/m^{-2}.s^{-1} and x=0.01 for different gravity levels: microgravity (0g), Moon gravity (0.16g), Mars gravity (0.38g), Earth gravity (1g)

5.1. *Gravity effect on bubble size distribution*

Interesting results were obtained concerning the effect of the gravity on the flow structure, especially in bubbly flows as shown in Figure 13 and in the video: https://www.esa.int/Enabling_Support/Space_Engineering_Technology/Just_add_bubbles_for_cooler_future_spacecraft.
Small bubbles are formed in the Preheater 2, and we can remark that the bubble sizes and

shapes are very sensitive to gravity. In microgravity and Moon gravity, the bubble sizes are larger than in Mars and Earth gravity. This is due to two effects. The sizes of the bubbles detaching from the wall of Preheater 2 are larger, since the bubbles are mainly detached by the shear of the flow and not by the buoyancy force, at least in microgravity. Moreover the rate of coalescence of the bubbles is higher in microgravity, as reported in previous studies [2, 15]. These 2 effects lead to larger bubble sizes. Bubbly flows in Mars gravity and earth gravity do not look very different. The bubble sizes and the bubble deformations are similar. It seems that a threshold in the gravity level between Moon and Mars, leads to a different behavior of the bubbly flow. We can see that in microgravity, the bubbles are spherical and they have a rectilinear trajectory. Even in Moon gravity, a small deformation of the bubbles can be seen. The deformation and oscillation of the bubbles are linked to their relative velocity due to buoyancy, which leads to detachment of eddies in their wake. These preliminary results concerning the effect of partial gravity (Moon and Mars) on the two-phase flow dynamics are of great interest and show that the flow structure cannot be predicted easily by interpolation of results obtained both in microgravity and earth gravity.

5.2. *Bubble radial distribution in the tube*

In order to check the axisymmetry of the two-phase flow, some experiments were performed on ground in vertical upward bubbly flow and during the parabolic flight campaign. On ground experiments, nucleate boiling was generated in the last part of the preheater 2 PH2.3 at 3 mass fluxes G=50, 100 and 150 kg/m^{-2}.s^{-1}. As mentioned previously for parabolic flight experiments, only PH2.1 was utilized. To analyse the bubble distributions in the tube, the power was limited in the preheater 2 and the quality x was lower than 0.01, to have a limited number of bubbles to ease the bubble detection and to avoid overlapping of several bubbles. The images of the 2 cameras are processed using Matlab software following the different steps (see Figure 14): starting from the raw image (a), substraction of a background image without bubble (b), enlightening of the bubbles (c), binarization (d), bubble filling (e), morphological opening (f), contour detection (g).

The space resolution of the cameras is 30 pixels/mm. From the contour of the bubble it is possible to determine the position of the center of gravity of the bubbles: longitudinal (x) and lateral (y) coordinates, their equivalent diameter (diameter of a disk with the same area). During the parabolic flight campaign, the bubble sizes were much larger in microgravity and in Moon gravity and too few bubbles are observed in the test section during the parabolas, to obtain a converged bubble lateral distribution after image processing. Thus, only the results concerning converged values of the mean bubble position and its RMS value for the experiments performed in Mars gravity are presented in Figure 15 and the radial distributions were calculated for a population of 700 bubbles. The mean lateral positions (y and z) of the bubbles in the tube and their rms values are reported in Table 4. We can see a slight asymmetry of the bubble distribution, which is confirmed by the mean values of the lateral position especially for the camera 2 for G=150 kg/m^{-2}.s^{-1}. Camera 2 has taken the images in the plane of the elbows, which is the most affected by the Dean vortices. Despite the use of PH2.1 in these experiments, it is interesting to see that for the lowest mass fluxes G=50 and 100 kg/m^{-2}.s^{-1}, the asymmetry of the distribution is not critical.

On ground experiments, in vertical upward flow, the third part of the prehater 2 PH2.3 was used. In this configuration, vapor bubbles are mostly produced at a distance 35 to 40 cm downstream the elbow, for which the single-phase flow has almost recovered its axisymmetry. The equivalent diameters of the bubbles ranged from 0.3 mm to 1.8 mm. About 2000 bubbles were detected in the processed images. The distributions of lateral position of the bubbles (y) on the 2 cameras are displayed in Figure 15. Bubbles are distributed quite in a homogeneous way over the pipe cross section. The mean distance is for most of the runs lower than 0.1 mm from the

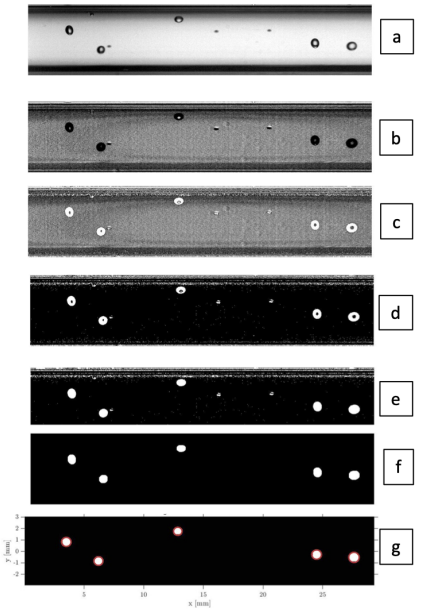

Figure 14. Different steps of image processing

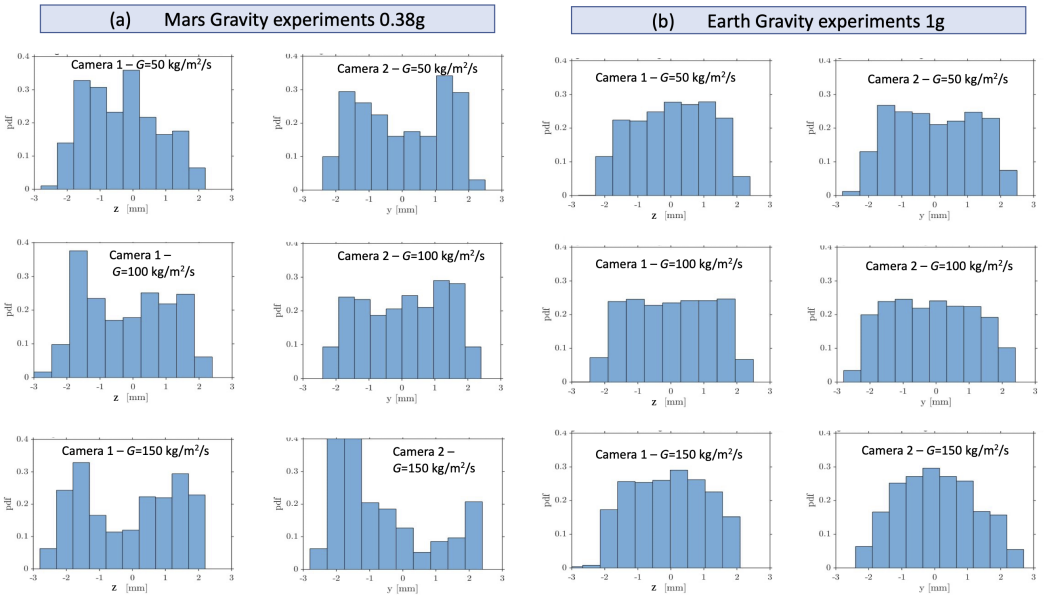

Figure 15. Bubble lateral distributions measured from the images of the 2 cameras: **(a)**: parabolic flight experiments in Mars Gravity 0.38g, **(b)**: Ground experiments in normal gravity 1g.

axis. Thus the bubble distributions can be considered as axisymmetric for bubbles formed in the preheaters at least 29 cm downstream the second elbow. Despite the limited length of the Preheater 2, for all the flow rates, the bubble lateral distributions are symmetrical, which validates

the design of the CoSmo breadboard.

Table 4. Bubble distribution

			cam 1	cam 1	cam 2	cam 2
G(kg/m^2/s)	Preheater 2	Gravity Level	mean pos.	rms pos.	mean pos.	rms pos.
50	PH2.1	0.38g	-0.32 mm	1.1 mm	0.0061 mm	1.3mm
100	PH2.1	0.38g	-0.19 mm	1.2 mm	0.069 mm	1.3 mm
150	PH2.1	0.38g	-0.11 mm	1.4 mm	-0.69 mm	1.4mm
50	PH2.3	1g	0.035 mm	1.1 mm	-0.004 mm	1.2mm
100	PH2.3	1g	0.029 mm	1.2 mm	-0.15 mm	1.3 mm
150	PH2.3	1g	-0.068 mm	1.1 mm	0.066 mm	1.2mm

6. Conclusion

In the frame of a project of the European Space Agency, a small scale flow boiling loop CoSmo has been designed in collaboration between the Institute of Fluid Mechanics of Toulouse and Airbus/ Defence and Space. Aiming at a potential implementation on-board the International Space Station, CoSmo has to fulfil typical size, power consumptions and weight constraints. The presence of singularities as elbows in the hydraulic circuit perturbes the flow hydrodynamics by creating Dean vortices and a strong flow asymmetry downstream the elbows. This perturbation is damped by viscous effects and after a decay length the flow recovers its axisymmetry. The objective of this study was to characterize the decay of the flow perturbation after two elbows both by PIV measurements and numerical simulations. The decay lengths obtained from numerical simulation and experiments are in good agreement for different flow Reynolds numbers Re_l equal to 500, 1000, 1500. For Re_l= 2000, the experimental value of the decay length is much smaller than the numerical one, probably because of the transition to a turbulent flow. From these results a design of the CoSmo loop was proposed. A preheater between the second elbow and the test section was composed of 3 heating parts to generate bubble vaporisation. For bubbly flows very sensitive to flow asymmetry, the downstream part of the preheater PH2.3 has to be used. The other parts of the preheater PH2.1 and PH2.2 can be used for flow with higher quality (slug flow or annular flows) less sensitive to the secondary flow downstream the elbows. The CoSmo loop was used to assess the axisymmetry of the bubble distributions in the test section thanks to 2 high-speed video cameras taken images in two perpendicular planes. Experiments were performed on ground in vertical upward flow and in partial gravity during a parabolic flight campaign. During the flight campaign only the preheater PH2.1 worked and a asymmetry of the bubble distribution was observed for the highest mass flux G=150 kg/m^{-2}.s^{-1}. For ground experiments, the preheater PH2.3 was used and the distribution of the bubbles was found symmetrical in the 2 planes for the 3 flow rates. For future experiments the test section will be replaced by a heated tube to study heat transfer coefficient in flow boiling. The CoSmo loop will allow to implement different test section and measurement techniques such as a sapphire tube using Pt 100 probes [15, 39] or temperature sensitive paint [19].

Conflicts of interest

The authors declare no competing financial interest.

Dedication

The manuscript was written through contributions of all authors. All authors have given approval to the final version of the manuscript.

Acknowledgments

Airbus DS and IMFT have been supported by the European Space Agency through the Invitation to Tender AO/1-9380/NL/KML. IMFT would like also to thank the french space agency CNES through the GDR "Micropesanteur Fondamentale et Appliquée" for additionnal support.

Supplementary data

Supporting information for this article is available on the ESA website.

References

[1] A. E. Dukler, J. A. Fabre, J. B. McQuillen, R. Vernon, "Gas-liquid flow at microgravity conditions: Flow patterns and their transitions", *Int. J. Multiphase Flow* **14** (1988), no. 4, p. 389-400.

[2] C. Colin, J. A. Fabre, A. E. Dukler, "Gas-liquid flow at microgravity conditions–I. Dispersed bubble and slug flow", *Int. J. Multiphase Flow* **17** (1991), no. 4, p. 533-544.

[3] L. Zhao, K. S. Rezkallah, "Gas-liquid flow patterns at microgravity conditions", *Int. J. Multiphase Flow* **19** (1993), no. 5, p. 751-763.

[4] W. S. Bousman, J. B. McQuillen, L. C. Witte, "Gas-liquid flow patterns in microgravity: Effects of tube diameter, liquid viscosity and surface tension", *Int. J. Multiphase Flow* **22** (1996), no. 6, p. 1035-1053.

[5] C. Colin, J. A. Fabre, J. McQuillen, "Bubble and slug flow at microgravity conditions: state of knowledge and open questions", *Chem. Eng. Commun.* **141-142** (1996), no. 1, p. 155-173.

[6] K. S. Rezkallah, "Weber number based flow-pattern maps for liquid-gas flows at microgravity", *Int. J. Multiphase Flow* **22** (1996), no. 6, p. 1265-1270.

[7] J.-f. Zhao, J. C. Xie, H. Lin, W. R. Hu, A. V. Ivanov, A. Y. Belyaev, "Experimental studies on two-phase flow patterns aboard the Mir space station", *Int. J. Multiphase Flow* **27** (2001), no. 11, p. 1931-1944.

[8] K. J. Elkow, K. S. Rezkallah, "Void fraction measurements in gas-liquid flow under $1g$ and μ conditions using capacitance sensors", *Int. J. Multiphase Flow* **23** (1997), no. 5, p. 815-829.

[9] L. Zhao, K. S. Rezkallah, "Pressure drop in gas-liquid flow at microgravity conditions", *Int. J. Multiphase Flow* **21** (1995), no. 5, p. 837-849.

[10] O. Haruhito, "Microgravity Heat Transfer in Flow Boiling", in *Advances in Heat Transfer*, vol. 37, Elsevier, 2003, p. 1-76.

[11] H. Zhang, I. Mudawar, M. M. Hasan, "CHF model for subcooled flow boiling in Earth gravity and microgravity", *Int. J. Heat Mass Transfer* **50** (2007), no. 19-20, p. 4039-4051.

[12] G. P. Celata, G. Zummo, "Flow boiling heat transfer in microgravity: recent progress", *Multiph. Sci. Technol.* **21** (2009), no. 3, p. 187-212.

[13] C. Baltis, G. P. Celata, M. Cumo, L. Saraceno, G. Zummo, "Gravity Influence on Heat Transfer Rate in Flow Boiling", *Microgravity Sci. Technol.* **24** (2012), no. 3, p. 203-213.

[14] H. Ohta, S. Baba, "Boiling Experiments Under Microgravity Conditions", *Exp. Heat Transf.* **26** (2013), no. 2-3, p. 266-295.

[15] M. Narcy, E. de Malmazet, C. Colin, "Flow boiling in tube under normal gravity and microgravity conditions", *Int. J. Multiphase Flow* **60** (2014), p. 50-63.

[16] S. Luciani, D. Brutin, C. Le Niliot, O. Rahli, L. Tadrist, "Flow Boiling in Minichannels Under Normal, Hyper-, and Microgravity: Local Heat Transfer Analysis Using Inverse Methods", *J. Heat Transfer* **130** (2008), no. 10, article no. 101502.

[17] C. Konishi, H. Lee, I. Mudawar, M. M. Hasan, H. K. Nahra, N. R. Hall, J. D. Wagner, R. L. May, J. R. Mackey, "Flow boiling in microgravity: Part 2 – Critical heat flux interfacial behavior, experimental data, and model", *Int. J. Heat Mass Transfer* **81** (2015), p. 721-736.

[18] Y. Zhang, B. Liu, J.-f. Zhao, Y. Deng, J. Wei, "Experimental Study of Subcooled Flow Boiling Heat Transfer on a Smooth Surface in Short-Term Microgravity", *Microgravity Sci. Technol.* **30** (2018), no. 6, p. 793-805.

[19] M. T. Lebon, C. F. Hammer, J. Kim, "Gravity effects on subcooled flow boiling heat transfer", *Int. J. Heat Mass Transfer* **128** (2019), p. 700-714.
[20] M. T. Lebon, C. F. Hammer, J. Kim, "Using a modified single-phase model to predict microgravity flow boiling heat transfer in the bubbly flow regime", *Exp. Heat Transf.* **34** (2021), no. 5, p. 474-492.
[21] J.-f. Zhao, "Two-phase flow and pool boiling heat transfer in microgravity", *Int. J. Multiphase Flow* **36** (2010), no. 2, p. 135-143.
[22] M. Narcy, C. Colin, "Two-phase flow in microgravity with and without phase change: recent progress and future prospects", *Interfacial Phenom. Heat Transf.* **3** (2015), no. 1, p. 1-17.
[23] C. Konishi, I. Mudawar, "Review of flow boiling and critical heat flux in microgravity", *Int. J. Heat Mass Transfer* **80** (2015), p. 469-493.
[24] K. Inoue, H. Ohta, H. Asano, O. Kawanami, R. Imai, K. Suzuki, Y. Shinmoto, T. Kurimoto, S. Matsumoto, "Heat Loss Analysis of Flow Boiling Experiments Onboard International Space Station with Unclear Thermal Environmental Conditions (2nd Report: Liquid-vapor Two-phase Flow Conditions at Test Section Inlet)", *Microgravity Sci. Technol.* **33** (2021), no. 5, article no. 57.
[25] V. S. Devahdhanush, S. J. Darges, I. Mudawar, H. K. Nahra, R. Balasubramaniam, M. M. Hasan, J. R. Mackey, "Flow visualization, heat transfer, and critical heat flux of flow boiling in Earth gravity with saturated liquid-vapor mixture inlet conditions – In preparation for experiments onboard the International Space Station", *Int. J. Heat Mass Transfer* **192** (2022), article no. 122890.
[26] V. P. Carey, *Liquid-Vapor Phase-Change Phenomena: An Introduction to the Thermophysics of Vaporization and Condensation Processes in Heat Transfer Equipment*, 2 ed., CRC Press, 2018.
[27] W. R. Dean, "XVI. Note on the motion of fluid in a curved pipe", *The London, Edinburgh, and Dublin Philosophical Magazine and Journal of Science* **4** (1927), no. 20, p. 208-223.
[28] W. R. Dean, J. M. Hurst, "Note on the motion of fluid in a curved pipe", *Mathematika* **6** (1959), no. 1, p. 77-85.
[29] S. A. Berger, L. Talbot, L. S. Yao, "Flow in Curved Pipes", *Annu. Rev. Fluid Mech.* (1983), p. 461-512.
[30] K. C. Cheng, F. P. Yuen, "Flow Visualization Studies on Secondary Flow Patterns in Straight Tubes Downstream of a 180 deg Bend and in Isothermally Heated Horizontal Tubes", *J. Heat Transfer* **109** (1987), no. 1, p. 49-54.
[31] J. A. Fairbank, R. M. C. So, "Upstream and downstream influence of pipe curvature on the flow through a bend", *Int. J. Heat Fluid Flow* **8** (1987), no. 3, p. 211-217.
[32] J. T. Ault, K. K. Chen, H. A. Stone, "Downstream decay of fully developed Dean flow", *J. Fluid Mech.* **777** (2015), p. 219-244.
[33] A. Pantokratoras, "Steady laminar flow in a 90° bend", *Adv. Mech. Eng.* **8** (2016), no. 9, p. 1-9.
[34] P. L. Spedding, E. Benard, G. M. Mcnally, "Fluid Flow through 90 Degree Bends", *Dev. Chem. Eng. Mineral Process.* **12** (2004), no. 1-2, p. 107-128.
[35] K. D. Arvanitis, D. Bouris, E. Papanicolaou, "Laminar flow and heat transfer in U-bends: The effect of secondary flows in ducts with partial and full curvature", *Int. J. Therm. Sci.* **130** (2018), p. 70-93.
[36] P. H. M. Bovendeerd, A. A. V. Steenhoven, F. N. V. D. Vosse, G. Vossers, "Steady entry flow in a curved pipe", *J. Fluid Mech.* **177** (1987), p. 233-246.
[37] R. Budwig, "Refractive index matching methods for liquid flow investigations", *Exp. Fluids* **17** (1994), no. 5, p. 350-355.
[38] Y. K. Agrawal, R. Sabbagh, S. Sanders, D. S. Nobes, "Measuring the Refractive Index, Density, Viscosity, pH, and Surface Tension of Potassium Thiocyanate (KSCN) Solutions for Refractive Index Matching in Flow Experiments", *J. Chem. Eng. Data* **63** (2018), no. 5, p. 1275-1285.
[39] P. O. Ayegba, J. Sebilleau, C. Colin, "Hydrodynamics of vertical upward and downward flow boiling in a millimetric tube", *Int. J. Multiphase Flow* **153** (2022), article no. 104120.